condensed matter

MDPI

Article

Magnetization Reversal in Concave Iron Nano-Superellipses

Emre Öncü and Andrea Ehrmann *

Faculty of Engineering and Mathematics, Bielefeld University of Applied Sciences, 33619 Bielefeld, Germany; emre.oencue@fh-bielefeld.de

* Correspondence: andrea.ehrmann@fh-bielefeld.de

Abstract: Square magnetic nanodots can show intentional or undesired shape modifications, resulting in superellipses with concave or convex edges. Some research groups also concentrated on experimentally investigating or simulating concave nano-superellipses, sometimes called magnetic astroids due to their similarity to the mathematical shape of an astroid. Due to the strong impact of shape anisotropy in nanostructures, the magnetization-reversal process including coercive and reversibility fields can be expected to be different in concave or convex superellipses than that in common squares. Here, we present angle-dependent micromagnetic simulations on magnetic nanodots with the shape of concave superellipses. While magnetization reversal occurs via meander states, horseshoe states or the 180° rotation of magnetization for the perfect square, depending on the angle of the external magnetic field, more complicated states occur for superellipses with strong concaveness. Even apparently asymmetric hysteresis loops can be found along the hard magnetization directions, which can be attributed to measuring minor loops since the reversibility fields become much larger than the coercive fields.

Keywords: nanostructure; iron; object-orientated micromagnetic framework (OOMMF); asymmetry; minor loop; coercive field; reversibility field

Citation: Öncü, E.; Ehrmann, A. Magnetization Reversal in Concave Iron Nano-Superellipses. *Condens. Matter* **2021**, *6*, 17. https://doi.org/10.3390/condmat6020017

Academic Editor: Carmine Attanasio

Received: 17 April 2021
Accepted: 11 May 2021
Published: 12 May 2021

1. Introduction

Ferromagnetic nanoparticles can be used in a broad range of applications, especially in data storage and spintronics [1–4], but also in energy devices, for drug delivery, and hyperthermia treatment [5–8]. In data storage, many research groups investigated round or square magnetic nanodots as a special shape of nanoparticles, often with round or square inplane symmetry, which often show magnetization reversal via vortex states, a behaviour that is advantageous for data storage due to the strongly reduced inplane stray fields [9–13]. Besides metallic magnetic nanodots, there are several ferri- or ferromagnetic metal oxides of which the energy band gaps can be tailored by varying the contents of different metal ions [14–16].

Other shapes of magnetic nanodots, reached intentionally or by undesired shape modifications due to the lithography process, show a broad range of different magnetization-reversal processes and magnetic states. Kasperski et al., for example, found out-of-plane stripe domains in two-dimensional nanodots with large anisotropy [17]. Double- or multi-vortex states were described by some groups [18–20]. Structures with open cores can show horseshoe states, onion states, and various other magnetic states [21–23].

For square iron nanodots, a large variety of magnetization-reversal processes were found depending on inplane dimensions and nanodot thickness [11]. Iron is of special interest for nanodots with lateral dimensions of a few hundred nanometers, since shape anisotropy and magnetocrystalline anisotropy have effects of similar strengths, so that the superposition of these anisotropies may result in several magnetic states that cannot be found in materials with very small or very large magnetocrystalline anisotropy, such as permalloy or cobalt, respectively, or in polycrystalline materials [11].

However, real nanodots are usually not perfectly shaped, but show shape deviations due to imperfections of the lithography process or other techniques [24–26]. Due to the strong influence of shape anisotropy in magnetic nanodots counteracting the magnetocrystalline anisotropy, such undesired shape modifications may influence the magnetization-reversal process and the technologically relevant parameters of coercive field and reversibility field. This does not mean that the transverse-magnetization component is equal to zero, but that there are no irreversible magnetization-reversal processes necessary to reach a transverse-magnetization component equal to zero. In this state, further increasing the external magnetic field leads to small rotations of magnetization, but no irreversible switches, and the full orientation along the external magnetic field could be reached without irreversible steps. On the other hand, intentional shape deviations can be used to stabilize a certain desired magnetic state [27].

Here we investigate the influence of concave deformations of the edges of a square nanodot, resulting in so-called superellipses, sometimes also called subellipses. The formula of such superellipses is

$$|x/a|^n + |y/b|^n = 1,$$

resulting in a diamond for $n = 1$ [28]. Here, a and b were chosen to be identical, enabling producing a square for $n = 1$, a circle for $n = 2$, superellipses with convex edges for $n > 1$, and superellipses with concave shapes (also called subellipses) for $n < 1$. The latter is the considered case here, testing values from $n = 1$ to $n = 0.5$.

Such superelliptic nanodots are sometimes also called astroid shapes, while the astroid is actually only gained for $n = 2/3$. They automatically occur in matrices of round antidots [29] or as antidot astroids [30], or they can be found in cross-junctions [31]. Some groups investigated antivortex evolution in Py astroid-shaped nanodots [32–35]. However, a systematic investigation of magnetization reversal in such shapes with varying values of n has, to the best of our knowledge, not yet been performed.

2. Materials and Methods

The simulations in this paper were accomplished in the object-orientated micromagnetic framework (OOMMF) [36]. Iron (Fe) was used as the probe material for all simulations, using the typical literature values of Fe: $M_{S,Fe} = 1700 \cdot 10^3$ A/m as magnetization at saturation, $A_{Fe} = 21 \cdot 10^{-12}$ J/m as exchange constant, and $K_{1,Fe} = 48 \cdot 10^3$ J/m^3 as cubic magnetocrystalline anisotropy constant [37]. The Gilbert damping constant was 0.5 (quasistatic case), the crystalline orientation was set to constant, with the easy cubic anisotropy axes along 0° and 90° corresponding to epitaxially grown nanostructures. This is in contrast to a previous investigation of square iron nanodots with arbitrary anisotropy orientation per cell [11], to enable investigating the effect of an epitaxial growth in addition to the modification of the sample shape, and thus the shape anisotropy.

All samples had the same particle width and height of 500 nm each, thickness of 5 nm, and cell size of 5 nm. The latter was slightly larger than the Fe exchange length of approx. 3.7 nm; previous studies showed no differences between experiments with cell sizes of 5 and 2.5 nm [12], so that the slightly increased cell size was chosen to reduce simulation time. The masks chosen for simulations were prepared in Photoshop, starting from a square (SE0) and adding increasing concave curvature to the edges until $n = 0.5$ was reached (SE90). The given numbers correspond to the curvature percentage implemented in Photoshop from 0° to 90°. Some of the samples are depicted in Figure 1 with the definition of the angles used in the simulation.

The external magnetic field was swept between ±200 mT, applied in angles between 0° and 90° in steps of 15°. Longitudinal (M_L) and transversal magnetization components (M_T) were calculated, and screenshots were taken during the magnetization-reversal processes. The hysteresis loops and six snapshots of the magnetization-reversal process per simulation are depicted in Supplementary Information.

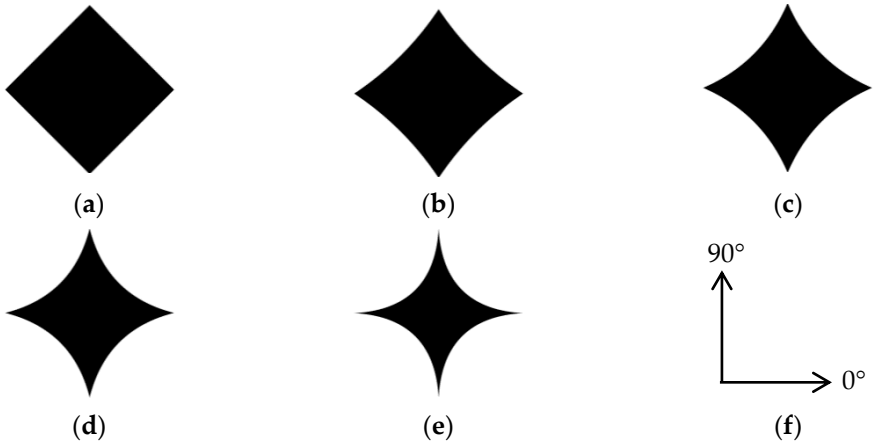

Figure 1. Sketches of some shapes under examination: (**a**) SE0; (**b**) SE20; (**c**) SE40; (**d**) SE60; and (**e**) SE90; (**f**) definition of angles in this study.

3. Results and Discussion

Figure 2 shows the hysteresis loops and magnetization reversal of some chosen angles, simulated for SE0. Snapshots were taken during magnetization reversal from positive to negative saturation. The colour of the snapshots represents the magnetization orientation in each position: red = magnetization pointing to the right, blue = magnetization pointing to the left, white = magnetization pointing from top to bottom or vice versa.

For field orientation of 0°, a typical easy axis hysteresis loop was visible (Figure 2a), correlated with magnetization reversal via a 180° switch (Figure 2b), as also indicated by the transverse-magnetization component (Figure 2a), which is continuously zero.

This was different for all other angles, as indicated by the partly relatively large transverse-magnetization components (Figure 2c,e) and the snapshots in Figure 2d,f. Generally, such large values of transverse magnetization indicate that, in the corresponding external magnetic-field ranges, large parts of magnetization were orientated perpendicular to the external magnetic field, as visible, e.g., in Figure 2d for −16 or −19 mT. Abrupt changes of the transverse (or longitudinal)-magnetization component indicate irreversible changes, such as the nucleation or vanishing of a domain wall and the coherent switching of parts of the magnetization. Identical values of longitudinal and transverse magnetization in a certain field range, e.g., in Figure 2e near −20 mT for the field sweep from positive to negative saturation, often indicate an approximately 45° orientation of magnetization, as visible in Figure 2f for −27 mT, but could also be related to much more complicated states, as visible in Figure 2f for −18 or −22 mT.

For an angle of 15°, magnetization reversal starts with a meander state (Figure 2d, −16 mT) into a state that could be described as an asymmetric horseshoe state (Figure 2d, −19 mT), before saturation is reached (−78 mT). These different states are correlated with steps or peaks in the longitudinal or transverse-magnetization component, respectively.

Here, and for many simulations along an angle that is not identical to a hard or easy axis of magnetization in the system, the relatively large external magnetic fields were not sufficient to fully set transverse magnetization to zero, since there is always a superposition between all anisotropies and the external magnetic field, defining the energetically favourable orientation of each elementary magnet. This also means that, by crossing the symmetry axis of a fourfold system, the sign of the residual transverse magnetization at large external magnetic fields changes, since magnetic moments are generally orientated between the external magnetic field and the next easy axis, which is on different sides of the external magnetic field when angles on different sides of a symmetry axis are compared.

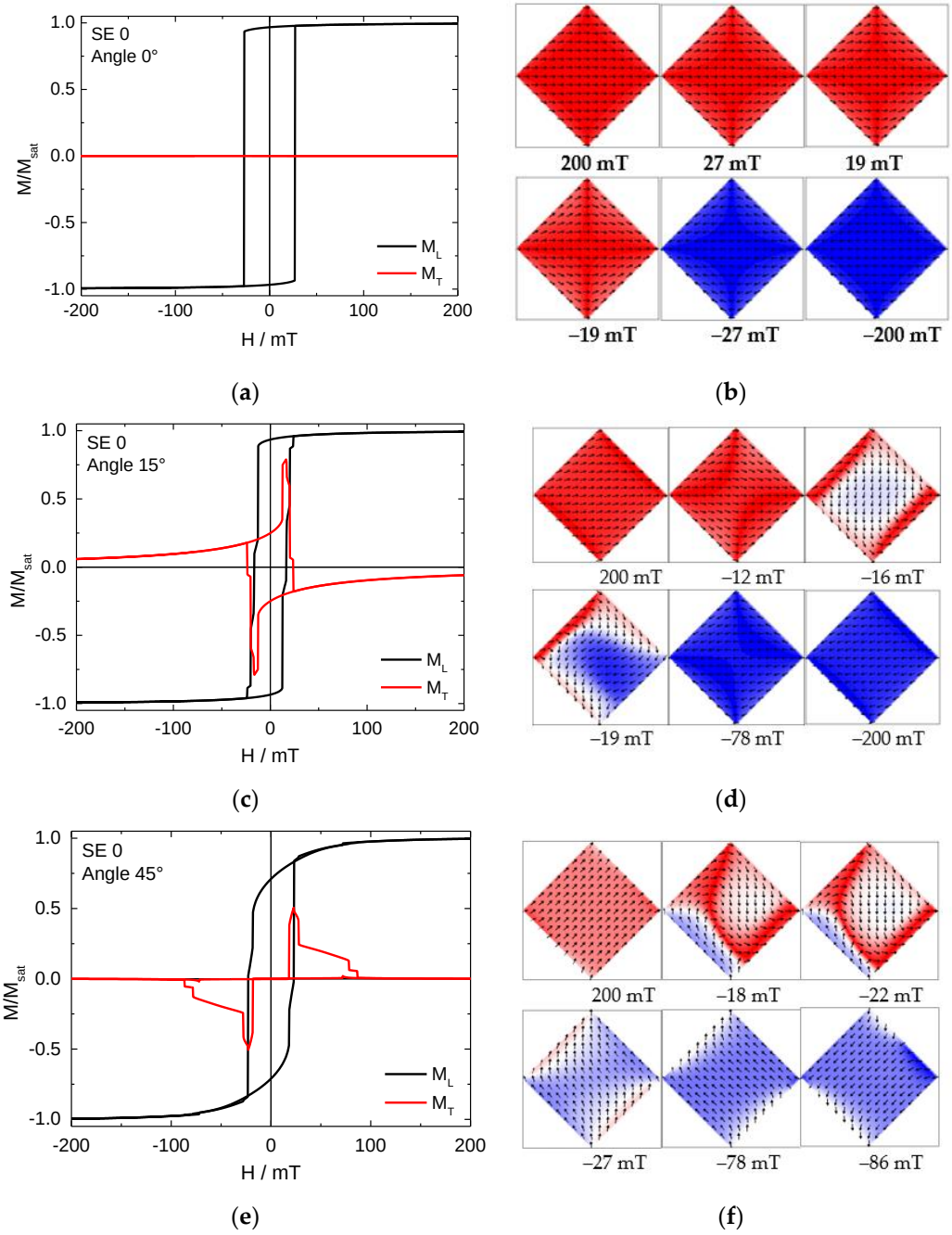

Figure 2. (**a**,**c**,**e**) Hysteresis loops and (**b**,**d**,**f**) snapshots of the magnetization reversal from positive to negative saturation and back, simulated for SE0 at angles defined in the graphs.

At an angle of 45°, there was again a visible asymmetric horseshoe (Figure 2f, −18 mT and −22 mT), which was transferred into a state with magnetization approximately 90° rotated from the original state (−27 mT). This behaviour sometimes occurs in magnetic thin-film samples with fourfold anisotropy; however, it is mostly known from exchange bias systems [38,39] and was not recognized in a previous investigation of sputtered square Fe nanodots [11]. This shows the influence of an epitaxial structure as compared to a polycrystalline one. Magnetization reversal via a 180° switch, visible in Figure 2b, was not found at all in the previous investigation of sputtered square Fe nanodots [11], underlining the importance of differentiating between sputtered and epitaxially grown nanodots, especially when defining suitable magnetic nanopatterns for storage applications.

Figure 3 depicts simulations of Sample SE20 at chosen angles. For an angle of 15° with respect to the external magnetic field, magnetization reversal occurred via 180° switching (Figure 3a,b); the same behaviour was found for 0° (not shown here).

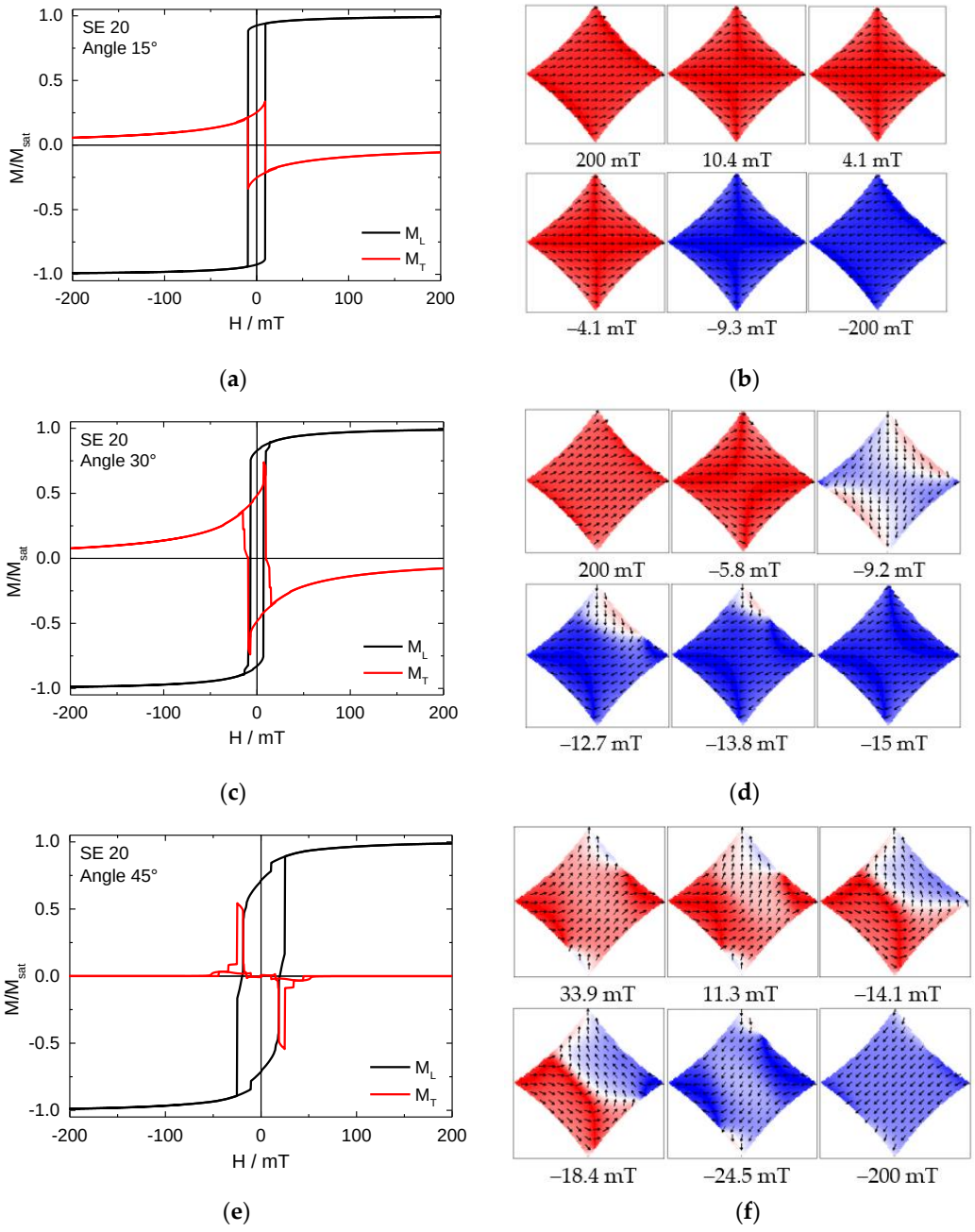

Figure 3. (**a**,**c**,**e**) Hysteresis loops and (**b**,**d**,**f**) snapshots of magnetization reversal from positive to negative saturation and back, simulated for Sample SE20 at angles defined in the graphs.

For 30°, magnetization reversal occurred via an intermediate state rotated by ~90° (Figure 3d, –9.2 mT) with respect to the relaxed state near remanence (−5.8 mT), followed by an asymmetric horseshoe state (−12.7 mT), before negative saturation was reached (−15 mT). For an angle of 45°, magnetization reversal started with a horseshoe state (Figure 3f, −14.1 and −18.4 mT), before magnetization was fully reversed.

This clear deviation between SE0 (SE10 shows similar behaviour) and SE20 indicates the influence of arbitrary or intentional modifications of the edges of the nanodots, allowing for modifying magnetization-reversal processes.

Simulated magnetization reversal for SE30 is partly depicted in Figure 4. While a similar 90° reversal via an intermediate state occurred for an angle of 30° (Figure 4b, −8.6 mT), as already found in Figures 2f and 3d, for an angle of 45°, a new state became visible with a nearly complete domain wall splitting the sample into two halves (Figure 4d, −32.5 mT). This state can be interpreted as an extreme horseshoe state. Contrary to the similar state visible in Figure 3f (−18.4 mT), magnetization near the corners here followed the shape anisotropy, i.e., pointed outwards. This means that this state could also be interpreted as similar to an antivortex state; however, in such an antivortex state, there would be a magnetic singularity in the particle, typically near the middle.

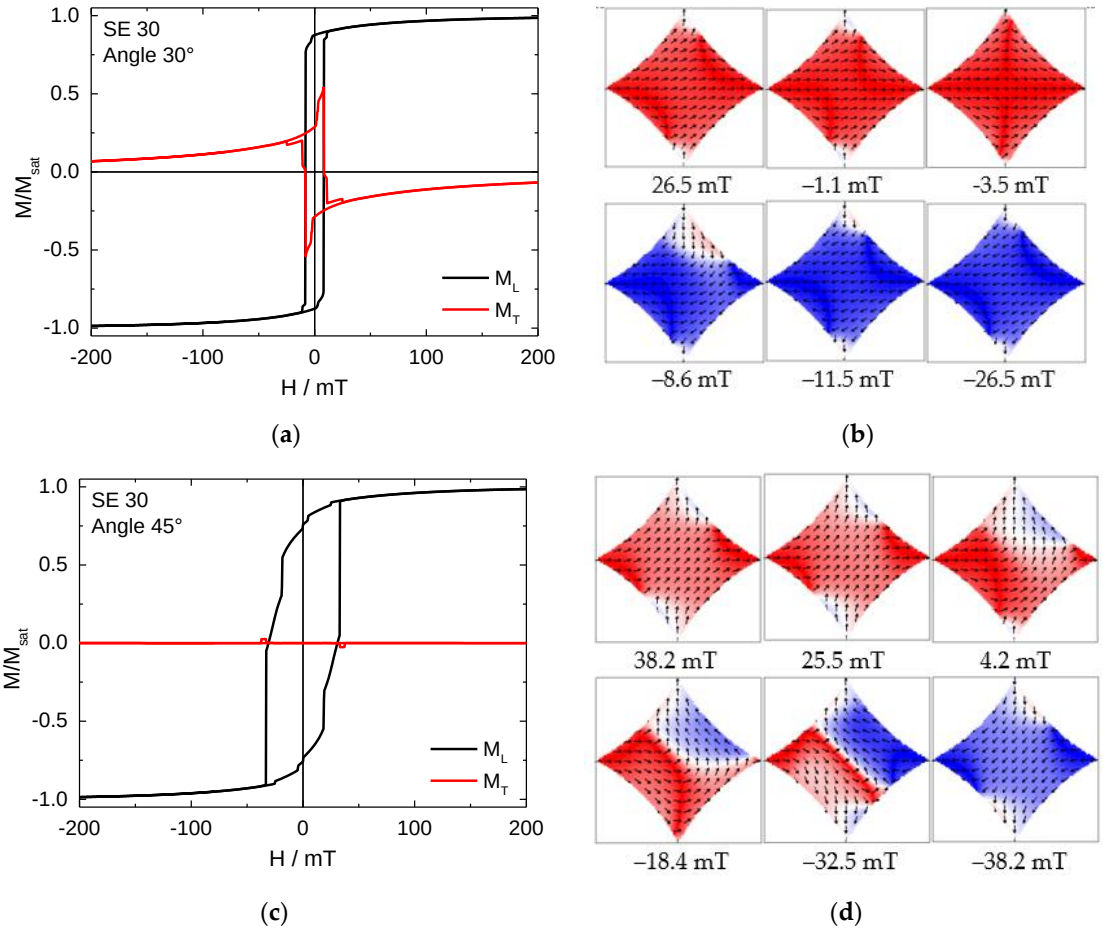

Figure 4. (**a**,**c**) Hysteresis loops and (**b**,**d**) snapshots of magnetization reversal from positive to negative saturation and back, simulated for SE30 at angles defined in the graphs.

While SE40 did not show new magnetization states, something unexpected happened in SE50, as shown in Figure 5. At an angle of 0°, an apparent asymmetry of the transverse-magnetization component was visible (ditto for 90°).

Such an asymmetry is typical for exchange bias systems [39]; however, it can also occur in single-material nanostructures in which the shape anisotropy creates magnetic hard and soft areas [40]. Here, this asymmetry is due to an even simpler reason. As shown in Figure 5b (15 mT), magnetization in both the "top" and the "bottom" corner pointed "downwards", i.e., there was an inherent asymmetry directly from the beginning. The sharper the corners became in this study, the stronger the shape anisotropy was there, and the larger the reversibility fields were, which were sufficient to create a fully symmetric saturated state.

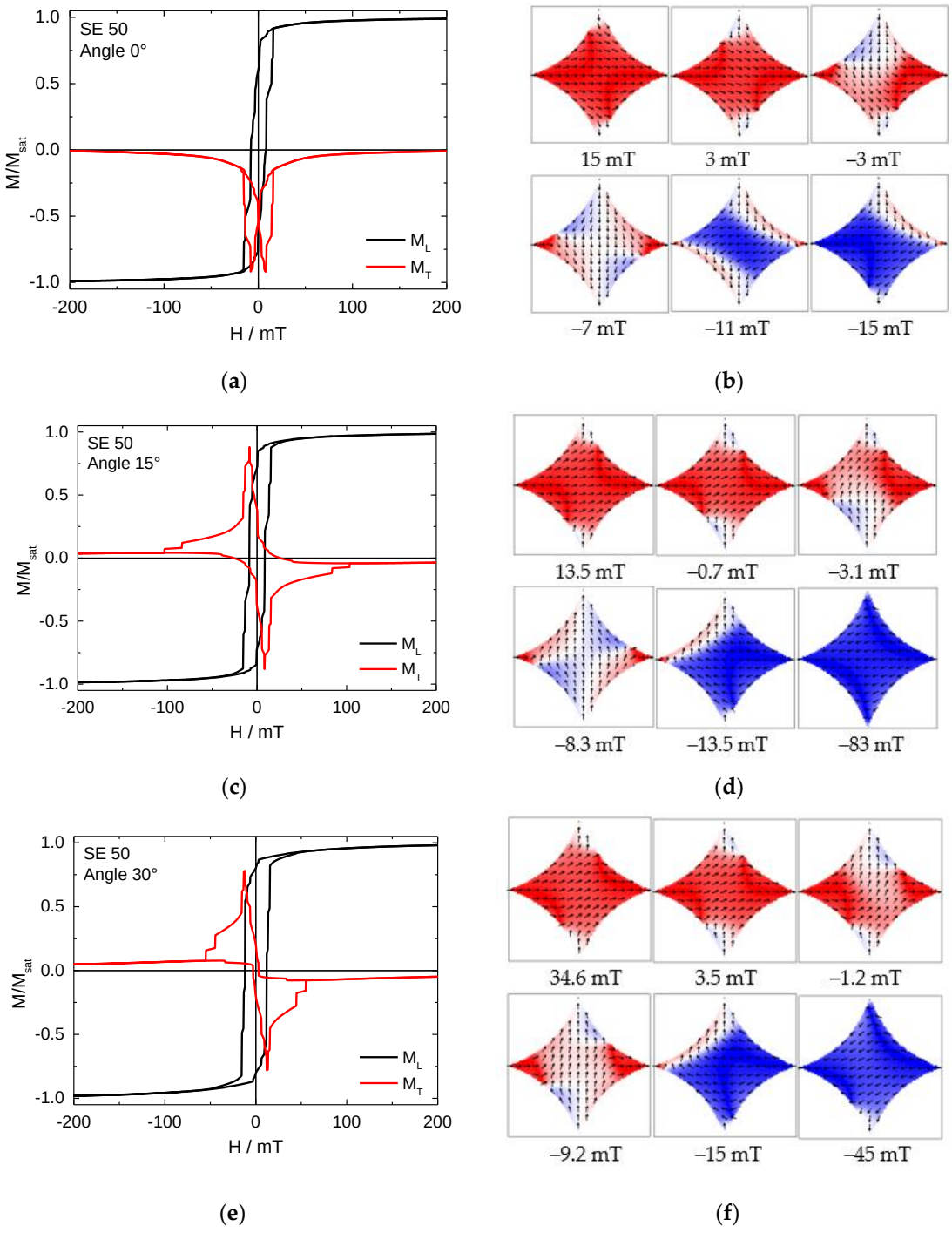

Figure 5. (**a**,**c**,**e**) Hysteresis loops and (**b**,**d**,**f**) snapshots of magnetization reversal from positive to negative saturation and back, simulated for SE50 at angles defined in the graphs.

To clarify this point, a minor loop was simulated here. While this can be of technological interest if properly recognized [40], this potential problem can occur in measurements where the transverse-magnetization component is often not available. Very often, measurements are performed in such a way that the range of the external magnetic field is restricted to approximately twice or three times that of the coercive field; here, a coercive field of 7.5 mT was in strong contrast with a reversal field larger than the maximal applied field of 200 mT.

However, this special situation of 0° often causes similar problems in simulations due to a perfectly symmetric shape of the nanodots under examination, but is in reality

nearly never met. Due to the combination of symmetries of magnetocrystalline and shape anisotropy, this effect was slightly larger here than that for simulations of polycrystalline nanodots [11]. While a slight sample rotation by $\pm 1^\circ$ in the latter is usually sufficient to break the symmetry, large reversibility fields were also visible here for larger sample rotations, as is shown in Figure 6.

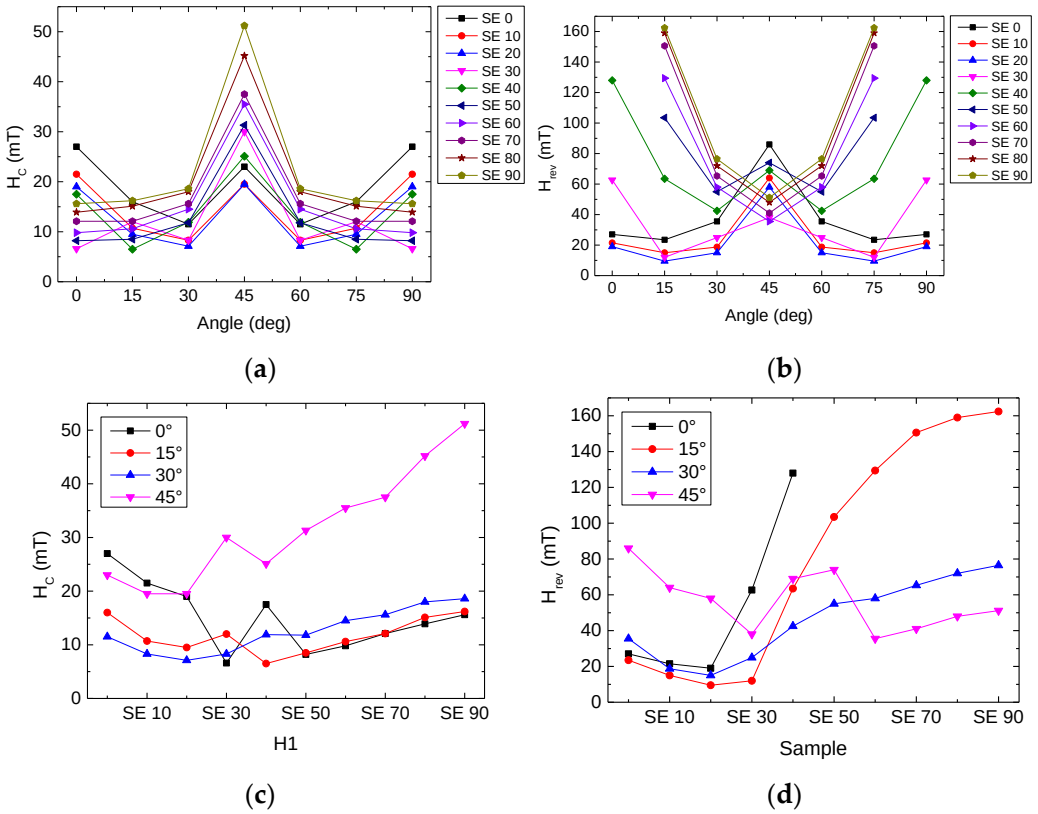

Figure 6. (**a**,**c**) Coercive fields and (**b**,**d**) reversibility fields as function of (**a**,**b**) the angle of the external magnetic field or (**c**,**d**) the sample number, respectively.

Larger angles (here: 15°, 30°) already indicated the increase in reversibility fields, which was nearly invisible in the longitudinal hysteresis loops, but well-visible in the transverse loops, and may in reality lead to measuring too narrow a field range, which may then result in undetected minor loops.

In residual Samples SE60 ... SE90, no new magnetic states occurred, and no full antivortex was visible.

For a quantitative comparison of the magnetization reversal of the samples under examination in this study, Figure 6 depicts coercive fields H_C and reversibility fields H_{rev} in the angular range of $0^\circ - 90^\circ$. Values in Figure 6a,c and Figure 6b,d were equal, depicted against the angles of the external magnetic field or the sample number. In most cases, 45° showed the highest coercive field, indicating that this orientation corresponds to an easy axis [41–43]. Deviations from this behaviour, as shown in Figure 6c by comparing 0° and 45° for Samples SE10 and SE20, can be attributed to the previously discussed high symmetry of the 0° orientation, which may suppress magnetization reversal, since no rotational direction is favoured by geometry or external magnetic field.

While there were a few visible trends, there were always values that did not correspond to these trends, typically due to changes in magnetization-reversal modes. The coercive fields were usually larger for $0^\circ/90^\circ$, i.e., the easy axes of the magnetocrystalline anisotropy, and for 45°, i.e., the easy axis of the shape anisotropy (Figure 6a), as shown by the magnetic states reaching near remanence for samples with strong edge curvature. The latter becomes

more important for larger sample numbers, i.e., stronger curvature, corresponding to a stronger impact of the shape anisotropy.

This is also visible in Figure 6c, where the coercive fields measured for a field orientation of 45° increase with increasing sample number, i.e., with stronger concave curvature of the edges. For the other angles, there is no clear trend visible in Figure 6c.

The angle-dependent reversibility fields (Figure 6b) showed a maximum at 45° for the small pure square and deviations from it; for Samples SE30 ... SE90, there WERE additional local or even absolute maxima at 0°/90°. the aforementioned large reversibility fields at 0° for samples with high curvature, leading to the asymmetry visible in Figure 5a, were clearly related to a highly symmetric situation that cannot be reached in reality; for samples with high curvature, the reversibility fields continuously grew from 45° to the 0°/90° orientations.

For the sample-dependent reversibility fields (Figure 6d), there was a strong increase in reversibility fields with increasing curvature for 0° and 15°, while 30° showed only a slight increase, and the 45° curve did not show a clear trend.

Comparing coercive fields and reversal fields, it is obvious that the modifications of the perfect square lead to an increase in the coercive field around 45° and an increase in the reversal field around 0°. Depending on the desired behaviour in a specific application, these findings can help to modify either the coercive fields or reversibility fields and tailor the system to the desired magnetization-reversal behaviour [40].

4. Conclusions

Micromagnetic simulations of concave iron nano-superellipses showed that the magnetization-reversal processes were modified by the interaction of magnetocrystalline and shape anisotropy, the latter of which became stronger with a stronger curvature of the nanodots edges. Contrary to previous reports in the literature, no antivortices occurred; instead, horseshoe, onion, and meander states were found.

A comparison of the coercive fields and reversibility fields showed that a stronger concave curvature resulted in an increase in the coercive field around 45° and in the reversibility field around 0°, thereby enabling tailoring the magnetic properties of such nanodots according to the desired application.

Supplementary Materials: The following are available online at https://www.mdpi.com/article/10.3390/condmat6020017/s1. Hysteresis loops and exemplary snapshots for all shapes and angles under investigation.

Author Contributions: Conceptualization, E.Ö. and A.E.; validation, E.Ö. and A.E.; investigation, E.Ö.; writing—original-draft preparation, A.E. and E.Ö.; writing—review and editing, E.Ö. and A.E.; visualization, E.Ö. and A.E. All authors have read and agreed to the published version of the manuscript.

Funding: This research received no external funding.

Institutional Review Board Statement: Not applicable.

Informed Consent Statement: Not applicable.

Data Availability Statement: All data produced during this study are available in Supplementary Information.

Conflicts of Interest: The authors declare no conflict of interest.

References

1. Reiss, G.; Hütten, A. Applications beyond data storage. *Nat. Mater.* **2005**, *4*, 725–726. [CrossRef] [PubMed]
2. Harada, M.; Kuwa, M.; Sato, R.; Teranishi, T.; Takahashi, M.; Maenosono, S. Cation Distribution in Monodispersed MFe_2O_4 (M = Mn, Fe, Co, Ni, and Zn) Nanoparticles Investigated by X-ray Absorption Fine Structure Spectroscopy: Implications for Magnetic Data Storage, Catalysts, Sensors, and Ferrofluids. *ACS Appl. Nano Mater.* **2020**, *3*, 8389–8402. [CrossRef]
3. Poornaprakash, B.; Ramu, S.; Subramanyam, K.; Kim, Y.; Kumar, M.; Reddy, M.S.P. Robust ferromagnetism of ZnO:(Ni + Er) diluted magnetic semiconductor nanoparticles for spintronic applications. *Ceram. Int.* **2021**. [CrossRef]

4. Almessiere, M.; Slimani, Y.; Guner, S.; Sertkol, M.; Korkmaz, A.D.; Shirsath, S.E.; Baykal, A. Sonochemical synthesis and physical properties of $Co_{0.3}Ni_{0.5}Mn_{0.2}Eu_xFe_{2-x}O_4$ nano-spinel ferrites. *Ultrason. Sonochem.* **2019**, *58*, 104654. [CrossRef] [PubMed]
5. Esfe, M.H.; Saedodin, S.; Mahian, O.; Wongwises, S. Efficiency of ferromagnetic nanoparticles suspended in ethylene glycol for applications in energy devices: Effects of particle size, temperature, and concentration. *Int. Commun. Heat Mass Transf.* **2014**, *58*, 138–146. [CrossRef]
6. Barbucci, R.; Pasqui, D.; Giani, G.; De Cagna, M.; Fini, M.; Giardino, R.; Atrei, A. A novel strategy for engineering hydrogels with ferromagnetic nanoparticles as crosslinkers of the polymer chains. Potential applications as a targeted drug delivery system. *Soft Matter* **2011**, *7*, 5558–5565. [CrossRef]
7. Abu-Bakr, A.F.; Zubarev, A.Y. Effect of ferromagnetic nanoparticles aggregation on magnetic hyperthermia. *Eur. Phys. J. Spec. Top.* **2020**, *229*, 323–329. [CrossRef]
8. Slimani, Y.; Unal, B.; Hannachi, E.; Selmi, A.; Almessiere, M.A.; Nawaz, M.; Baykal, A.; Ercan, I.; Yildiz, M. Frequency and dc bias voltage dependent dielectric properties and electrical conductivity of $BaTiO_3$-$SrTiO_3$/$(SiO_2)_x$ nanocomposites. *Ceram. Int.* **2019**, *45*, 11989–12000. [CrossRef]
9. Mejía-López, J.; Altbir, D.; Romero, A.H.; Batlle, X.; Roshchin, I.V.; Li, C.-P.; Schuller, I.K. Vortex state and effect of anisotropy in sub-100-nm magnetic nanodots. *J. Appl. Phys.* **2006**, *100*, 104319. [CrossRef]
10. Noske, M.; Stoll, H.; Fähnle, M.; Gangwar, A.; Woltersdorf, G.; Slavin, A.; Weigand, M.; Dieterle, G.; Förster, J.; Back, C.H.; et al. Three-dimensional character of the magnetization dynamics in magnetic vortex structures: Hybridization of flexure gyromodes with spin waves. *Phys. Rev. Lett.* **2016**, *117*, 037208. [CrossRef] [PubMed]
11. Ehrmann, A.; Blachowicz, T. Systematic study of magnetization reversal in square Fe nanodots of varying dimensions in different orientations. *Hyperfine Interact.* **2018**, *239*, 48. [CrossRef]
12. Ehrmann, A.; Blachowizc, T. Vortex and double-vortex nucleation during magnetization reversal in Fe nanodots of different dimensions. *J. Magn. Magn. Mater.* **2019**, *475*, 727–733. [CrossRef]
13. Döpke, C.; Grothe, T.; Steblinski, P.; Klöcker, M.; Sabantina, L.; Kosmalska, D.; Blachowicz, T.; Ehrmann, A. Magnetic Nanofiber Mats for Data Storage and Transfer. *Nanomaterials* **2019**, *9*, 92. [CrossRef] [PubMed]
14. Almessiere, M.; Slimani, Y.; Güner, S.; Nawaz, M.; Baykal, A.; Aldakheel, F.; Akhtar, S.; Ercan, I.; Belenli, I.; Ozçelik, B. Magnetic and structural characterization of Nb^{3+}-substituted $CoFe_2O_4$ nanoparticles. *Ceram. Int.* **2019**, *45*, 8222–8232. [CrossRef]
15. Almessiere, M.; Slimani, Y.; Korkmaz, A.; Taskhandi, N.; Sertkol, M.; Baykal, A.; Shirsath, S.E.; Ercan, I.; Ozçelik, B. Sonochemical synthesis of Eu3+ substituted $CoFe_2O_4$ nanoparticles and their structural, optical and magnetic properties. *Ultrason. Sonochem.* **2019**, *58*, 104621. [CrossRef] [PubMed]
16. Sathisha, I.C.; Manjunatha, K.; Angadi, V.J.; Reddy, R.K. Structural, Microstructural, Electrical, and Magnetic Properties of $CuFe_{2-(x+y)}EuxSc_yO_4$ (where x and y vary from 0 to 0.03) Nanoparticles. *J. Supercond. Novel Magn.* **2020**, *33*, 3963–3973. [CrossRef]
17. Kasperski, M.; Puszkarski, H.; Hoang, D.-T.; Diep, H.T. Magnetic properties of two-dimensional nanodots: Ground state and phase transition. *AIP Adv.* **2013**, *3*, 122121. [CrossRef]
18. Vavassori, P.; Zaluzec, N.; Metlushko, V.; Novosad, V.; Ilic, B.; Grimsditch, M. Magnetization reversal via single and bouble vortex states in submicron Permalloy ellipses. *Phys. Rev. B* **2004**, *69*, 214404. [CrossRef]
19. Guslienko, K.Y.; Buchanan, K.S.; Bader, S.D.; Novosad, V. Dynamics of coupled vortices in layered magnetic nanodots. *Appl. Phys. Lett.* **2005**, *86*, 223112. [CrossRef]
20. Prosandeev, S.; Bellaiche, L. Controlling Double Vortex States in Low-Dimensional Dipolar Systems. *Phys. Rev. Lett.* **2008**, *101*, 097203. [CrossRef] [PubMed]
21. Vavassori, P.; Grimsditch, M.; Novosad, V.; Metlushko, V.; Ilic, B. Metastable states during magnetization reversal in square permalloy rings. *Phys. Rev. B* **2003**, *67*, 134429. [CrossRef]
22. Remhof, A.; Schumann, A.; Westphalen, A.; Last, T.; Kunze, U.; Zabel, H. Dipolar interactions in periodic arrays of rectangular ferromagnetic islands. *J. Magn. Magn. Mater.* **2007**, *310*, e794–e796. [CrossRef]
23. Zabel, H.; Schumann, A.; Westphalen, A.; Remhof, A. Order and Frustration in Artificial Magnetic Patterns. *Acta Phys. Pol. A* **2009**, *115*, 59–63. [CrossRef]
24. Gao, X.; Liu, L.; Birajdar, B.; Ziese, M.; Lee, W.; Alexe, M.; Hesse, D. High-Density Periodically Ordered Magnetic Cobalt Ferrite Nanodot Arrays by Template-Assisted Pulsed Laser Deposition. *Adv. Funct. Mater.* **2009**, *19*, 3450–3455. [CrossRef]
25. Li, Z.; Gao, S.; Brand, U.; Hiller, K.; Hahn, S.; Hamdana, G.; Peiner, E.; Wolff, H.; Bergmann, D. Nanomechanical character-ization of vertical nanopillars using an MEMS-SPM nano-bending testing platform. *Sensors* **2019**, *19*, 4529. [CrossRef] [PubMed]
26. Ehrmann, A.; Blachowicz, T.; Komraus, S.; Nees, M.-K.; Jakobs, P.-J.; Leiste, H.; Mathes, M.; Schaarschmidt, M. Magnetic properties of square Py nanowires: Irradiation dose and geometry dependence. *J. Appl. Phys.* **2015**, *117*, 173903. [CrossRef]
27. Blachowicz, T.; Ehrmann, A.; Steblinski, P.; Palka, J. Directional-dependent coercivities and magnetization reversal mechanisms in fourfold ferromagnetic systems of varying sizes. *J. Appl. Phys.* **2013**, *113*, 013901. [CrossRef]
28. Huang, W.W.; Li, Y.Y.; Niklas, K.J.; Gielis, J.; Ding, Y.Y.; Cao, L.; Shi, P.J. A superellipse with deformation and its application in describing the cross-sectional shapes of a square bamboo. *Symmetry* **2020**, *12*, 2073. [CrossRef]
29. Castán-Guerrero, C.; Herrero-Albillos, J.; Bartolomé, J.; Rodríguez, L.A.; Magén, C.; Kronast, F.; Gawronski, P.; Chubykalo-Fesenko, O.; Merazzo, K.J.; Vavassori, P.; et al. Magnetic antidot to dot crossover in Co and Py nanopatterned thin films. *Phys. Rev. B* **2014**, *89*, 144405. [CrossRef]

30. Sudsom, D.; Ehrmann, A. Micromagnetic Simulations of Fe and Ni Nanodot Arrays Surrounded by Magnetic or Non-Magnetic Matrices. *Nanomaterials* **2021**, *11*, 349. [CrossRef]
31. Janutka, A.; Gawronski, P. Spin-Transfer Driven Dynamics of Magnetic Vortices and Antivortices in Dots with Crystalline Cubic Anisotropy. *IEEE Trans. Magn.* **2017**, *53*, 1. [CrossRef]
32. Wang, H.; Campbell, C.E. Spin dynamics of a magnetic antivortex: Micromagnetic simulations. *Phys. Rev. B* **2007**, *76*, 220407. [CrossRef]
33. Xing, X.J.; Yu, Y.P.; Wu, S.X.; Xu, L.M.; Li, S.W. Bloch-point-mediated magnetic antivortex core reversal triggered by sudden excitation of a suprathreshold spin-polarized current. *Appl. Phys. Lett.* **2008**, *93*, 202507. [CrossRef]
34. Gliga, S.; Hertel, R.; Schneider, C.M. Switching a magnetic antivortex core with ultrashort field pulses. *J. Appl. Phys.* **2008**, *103*, 7. [CrossRef]
35. Gliga, S.; Yan, M.; Hertel, R.; Schneider, C.M. Ultrafast dynamics of a magnetic antivortex: Micromagnetic simulations. *Phys. Rev. B* **2008**, *77*, 060404. [CrossRef]
36. Donahue, M.J.; Porter, D.G. *OOMMF User's Guide, Version 1.0*; National Institute of Standards and Technology (NIST): Gaithersburg, MD, USA, 1999.
37. Kneller, E.F.; Hawig, R. The exchange-spring magnet: A new material principle for permanent magnets. *IEEE Trans. Magn.* **1991**, *27*, 3588–3560. [CrossRef]
38. Tillmanns, A.; Blachowicz, T.; Fraune, M.; Güntherodt, G.; Schuller, I.K. Anomalous magnetization reversal mechanism in unbiased Fe/FeF2 investigated by means of the magneto-optic Kerr effect. *J. Magn. Magn. Mater.* **2009**, *321*, 2932–2935. [CrossRef]
39. Blachowicz, T.; Ehrmann, A. Exchange Bias in Thin Films—An Update. *Coatings* **2021**, *11*, 122. [CrossRef]
40. Detzmeier, J.; Königer, K.; Blachowicz, T.; Ehrmann, A. Asymmetric hysteresis loops in structured ferromagnetic nanoparticles with hard/soft areas. *Nanomaterials* **2021**, *11*, 800. [CrossRef] [PubMed]
41. Grimsditch, M.; Hoffmann, A.; Vavassori, P.; Shi, H.T.; Lederman, D. Exchange-induced anisotropies at ferromagnetic-antiferromagnetic interfaces above and below the Néel temperature. *Phys. Rev. Lett.* **2003**, *90*, 257201. [CrossRef] [PubMed]
42. Pardavi-Horvath, M.; Ross, C.; McMichael, R. Shape effects in the ferromagnetic resonance of nanosize rectangular permalloy arrays. *IEEE Trans. Magn.* **2005**, *41*, 3601–3603. [CrossRef]
43. Blachowicz, T.; Tillmanns, A.; Fraune, M.; Ghadimi, R.; Beschoten, B.; Güntherodt, G. Exchange bias in epitaxial CoO/Co bilayers with different crystallographic symmetries. *Phys. Rev. B* **2007**, *75*, 054425. [CrossRef]